


Mapping of Lattice Strain in 4H-SiC Crystals by Synchrotron Double-Crystal X-ray Topography

JIANQIU GUO ^{1,3} YU YANG,^{1,4} BALAJI RAGHOTHAMACHAR,^{1,5}
MICHAEL DUDLEY,^{1,6} and STANISLAV STOUPIN^{2,7}

1.—Department of Materials Science and Engineering, Stony Brook University, Stony Brook, NY 11794, USA. 2.—Cornell High Energy Synchrotron Source, Cornell University, Ithaca, NY 14850, USA. 3.—e-mail: jqguo123@gmail.com. 4.—e-mail: yu.yang@stonybrook.edu. 5.—e-mail: balaji.raghothamachar@stonybrook.edu. 6.—e-mail: michael.dudley@stonybrook.edu. 7.—e-mail: stoupin@cornell.edu

The presence of lattice strain in *n*-doped 4H-SiC substrate crystals grown by a physical vapor transport method can strongly influence the performance of related power devices that are fabricated on them. Information on the level and the variation of lattice strain in these wafer crystals is thus important. In this study, a non-destructive method is developed based on synchrotron double-crystal x-ray topography to map lattice strains in 4H-SiC wafers. Measurements are made on two 4H-SiC substrate crystals—one is an unprocessed commercial wafer while the other was subject to a post-growth high-temperature heat treatment. Maps of different strain components are generated from the equi-misorientation contour maps recorded using synchrotron monochromatic radiation. The technique is demonstrated to be a powerful tool in estimating strain fields in 4H-SiC crystals. Analysis of the strain maps also shows that the normal strain components vary much more significantly than do the shear/rotation components, indicating that lattice dilation/compression rather than lattice tilt is the major type of deformation caused by both the incorporation of nitrogen dopants and the nucleation of basal plane dislocations.

Key words: Silicon carbide, double-crystal x-ray topography, lattice strain

INTRODUCTION

Residual stress is often observed in *n*-doped 4H-SiC substrate crystals after physical vapor transport (PVT) growth and/or high-temperature heat treatments. Since perfect crystals should be free of stress at a homogeneous temperature, the presence of residual stress at room temperature is usually a result of lattice strain brought about by the existence of lattice imperfections such as inhomogeneous distribution of point defects/dopants, dislocations, low-angle grain boundaries, precipitates, inclusions, etc. Such lattice strain will have a significant impact on the homogeneity of the epitaxial layers grown subsequently, thus affecting the

functionality and reliability of the related device structures.¹ It is therefore important to estimate the level and variation of lattice strain in these crystals. Double-crystal x-ray topography is a highly strain-sensitive technique for imaging single crystals.² With angular resolutions as low as a few seconds of arc, the technique yields a strain sensitivity of 10^{-6} level. Stress/strain measurements based on this technique have already been successfully applied to different single-crystal systems such as Si,³ GaAs,^{4,5} Nb,⁶ CdZnTe,⁷ InP,⁸ diamond^{9,10} which are primarily single crystals with cubic structures. In this study, we demonstrate that this technique is also extremely useful in estimating the strain level in highly anisotropic 4H-SiC substrate crystals.

(Received July 13, 2017; accepted September 1, 2017)

THEORY

When a single crystal is illuminated by monochromatic x-ray radiation of a certain divergence, only a limited region will diffract. This is due to the existence of lattice deformation (effective misorientation) that deviates the rest of the crystal from perfect Bragg condition by $\Delta\omega$, and thus only a small region is accepted for diffraction. With a single exposure, a so-called equi-misorientation contour can be obtained on the recording plate, as shown in Fig. 1a. In order to image the rest of the crystal, a small rotation of the same amount $\Delta\omega$ about the ω axis is applied to the crystal so that a different region will be accepted for diffraction and another contour will be obtained, as shown in Fig. 1b. A contour map can therefore be generated by rocking the crystal through the perfect Bragg condition with small steps of angular rotation and taking an exposure at each step. According to Bragg's Law, for an arbitrary location in the crystal referenced to a perfect lattice, the deviation from perfect Bragg condition is due to the convoluted effect of local lattice dilation/compression ($\partial u_i/\partial x_i$) and lattice shear/rotation ($\partial u_i/\partial x_k$). This can be expressed in the following equation⁶:

$$\omega^{x_i}(x_j) = \frac{\partial u_i}{\partial x_i} \tan \theta_B + \frac{\partial u_i}{\partial x_k} \quad (1)$$

where $\omega^{x_i}(x_j)$ denotes the angular deviation from perfect Bragg condition and, if a reference point is selected in the crystal to be free of strain, $\omega^{x_i}(x_j)$ equals the amount of angular movement one has to apply to shift the equi-misorientation contour from the reference point to the location of interest by rotating the diffracting plane x_i about x_j axis. θ_B is the perfect Bragg angle. In order to deconvolute these two strain components, an additional contour map is needed with diffraction taking place on the same lattice plane but with an opposite diffraction vector ($-\vec{g}$). This can be done practically by first rotating the crystal about the diffraction plane normal by 180° and recording another contour map in the same manner. In the $-\vec{g}$ contour map, the local deviation from perfect Bragg's condition is given by:

$$\omega^{-x_i}(x_j) = \frac{\partial u_i}{\partial x_i} \tan \theta_B - \frac{\partial u_i}{\partial x_k} \quad (2)$$

where the shear/rotation component $\partial u_i/\partial x_k$ makes an opposite contribution to the deviation in the $-\vec{g}$ map and thus has a negative sign in front of it. Simple addition and subtraction of Eqs. 1 and 2 yield:

$$\frac{\partial u_i}{\partial x_i} = \frac{\omega^{x_i}(x_j) + \omega^{-x_i}(x_j)}{2 \tan \theta_B} \quad (3)$$

$$\frac{\partial u_i}{\partial x_k} = \frac{\omega^{x_i}(x_j) - \omega^{-x_i}(x_j)}{2} \quad (4)$$

The values of these two strain components for any location in the crystal can thus be quantitatively estimated. The complete set of strain tensors ($\epsilon_{ij} = 1/2(\partial u_i/\partial x_j + \partial u_j/\partial x_i)$) can be accessed from various $\pm\vec{g}$ contour maps which are obtained by rotating different diffracting planes about different axes.

EXPERIMENTAL

In this study, two different silicon carbide samples were analyzed. The first sample was a 75-mm *n*-doped 4H-SiC commercial wafer. Synchrotron Monochromatic x-ray topography was carried out at Beamline 1-BM in the Advanced Photon Source (APS) in the Argonne National Laboratory. A double-crystal setup with a Bragg/Bragg+− setting was used in which the first crystal was a highly asymmetric Si (331) beam expander and the second crystal, the silicon carbide wafer, was diffracting with $\vec{g} = (0008)$ in reflection geometry.¹¹ A schematic of the diffraction geometry is shown in Fig. 2a. The $+\vec{g}$ contour map was obtained by rocking the wafer about the $[\bar{1}100]$ axis through the perfect Bragg condition and the $-\vec{g}$ map was obtained in the same fashion after the wafer was rotated about the $[0001]$ axis by 180° . The diffraction image was recorded on high-resolution x-ray films which were placed 30 cm from the sample and parallel with the sample surface for minimum image distortion. The sample was mounted on the motorized goniometer without adhesive tape so that no additional stress was applied to the wafer during the experiment.

The second sample we analyzed was a 5 mm × 5 mm piece cut from a 150-mm *n*-doped 4H-SiC commercial wafer. This sample was subject to a special high-temperature heat treatment in which a large thermal gradient was created by heating the sample on a local spot up to 1600°C . A high strain center was expected in this sample. Synchrotron monochromatic x-ray topography was carried out at Beamline C1 in the Cornell High Energy Synchrotron Source (CHESS). A similar double crystal set-up¹⁰ was used except that the sample was diffracting in transmission geometry, as shown in Fig. 2b. Two sets of $\pm\vec{g}$ contour maps were recorded; the diffraction vectors were $(11\bar{2}0)$ and $(\bar{1}100)$, respectively. For both measurements, the same orthogonal coordinate system is used where the x_1 , x_2 , and x_3 axis represents $[11\bar{2}0]$, $[\bar{1}100]$ and $[0001]$ crystal direction, respectively.

RESULTS AND DISCUSSION

Figure 3a and b shows the 0008 and 000 $\bar{8}$ contour maps recorded from the 75-mm 4H-SiC commercial wafer. The reference point (marked in red) is selected in the very center of the wafer and assumed

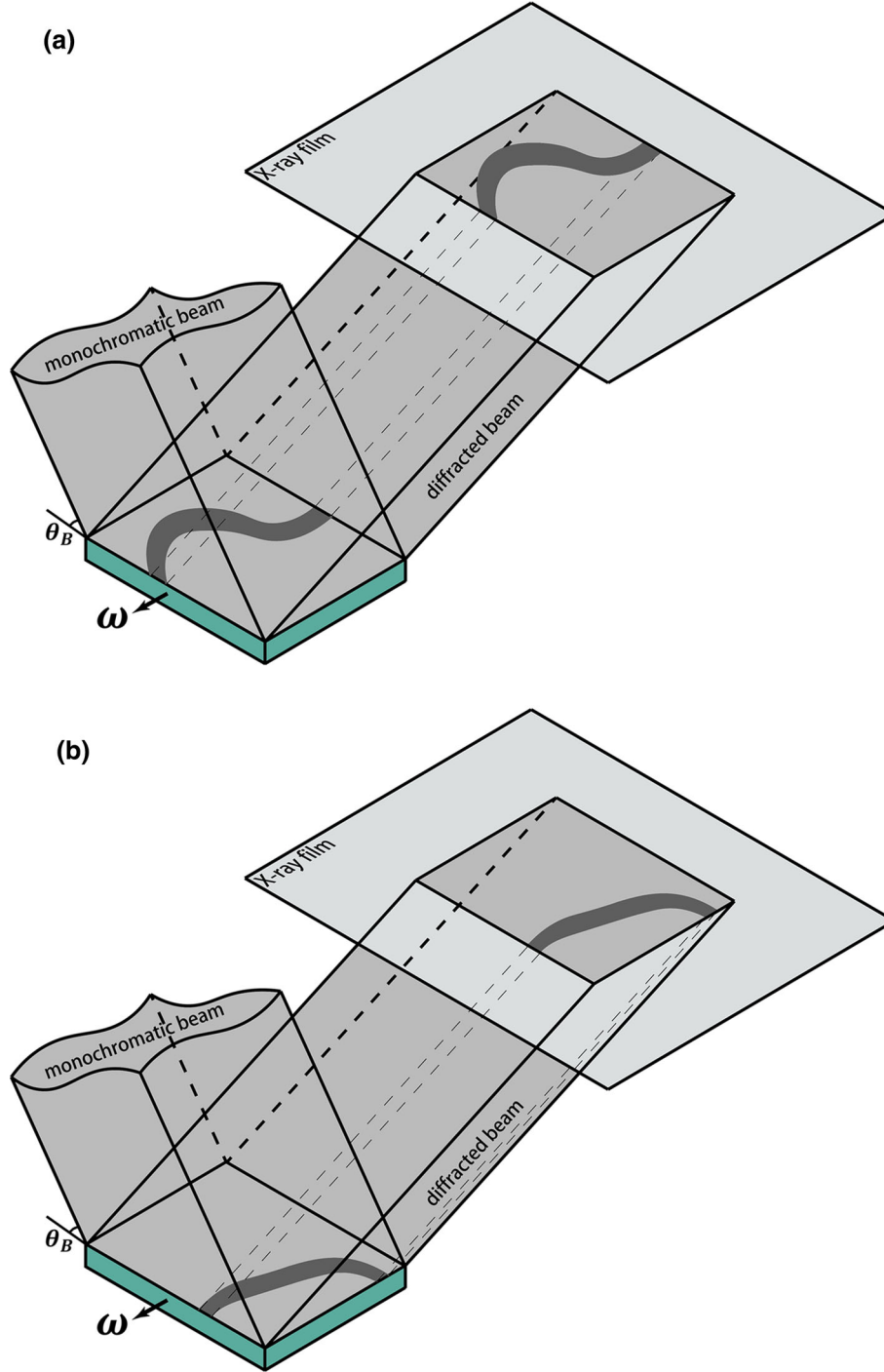


Fig. 1. (a) Equi-misorientation contour is obtained when the crystal is illuminated by monochromatic radiation but only a limited region diffracts. (b) When the crystal is rotated with a tiny step $\Delta\omega$ about ω axis, another region reaches Bragg condition and diffracts, making the contour shift to a different position.

to be free of strain. In both maps, adjacent contours are 3.6 s of arc in angular rotation from each other. In order to extract quantitative information, each contour map is divided into large numbers of small square boxes of equal size (more than 6000 boxes in the current case). Each box is identified with the value of angular rotation difference between the

region where the box is located and the region where the reference point is located. Therefore, two quantitative maps of angular rotation can be generated from $+\vec{g}$ and $-\vec{g}$ contour maps, respectively ($\omega^{x_3(x_2)}$ and $\omega^{-x_3(x_2)}$ in this case). Values of strain components $\partial u_3/\partial x_3$ and $\partial u_3/\partial x_1$ for any location in the wafer can be estimated via Eqs. 3 and 4.

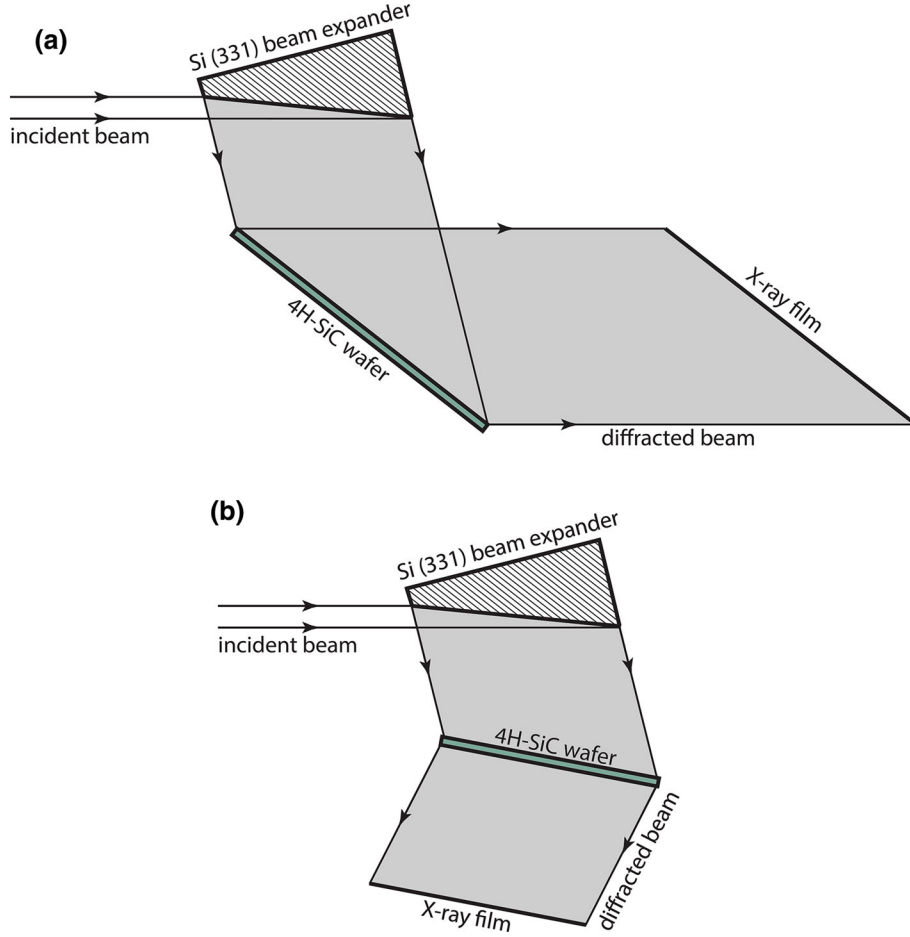


Fig. 2. Geometric set-ups for double-crystal x-ray topography in (a) reflection mode (APS) and (b) transmission mode (CHESS).

Corresponding strain maps are then plotted using MATLAB[®] and shown in Fig. 4.

In Fig. 4a, $\partial u_3 / \partial x_3$ shows a significant variation across the 75-mm wafer. With the reference point at the center of the wafer, the relative strain value ranges from -1.578×10^{-4} in the bottom right to 1.429×10^{-4} in the top left. $\partial u_3 / \partial x_3$ is equivalent to the normal strain component ϵ_{33} , which represents the dilation or compression in the lattice parameter, c . It is obvious that the variation of ϵ_{33} matches very well with the distribution of the contours, indicating that in 0008 reflection, the lattice dilation/compression makes a predominant contribution to the local deviation from perfect Bragg condition. In contrast, the level of strain component $\partial u_3 / \partial x_1$ is almost two orders of magnitude lower ($\sim 10^{-6}$ which is close to the sensitivity limit). Under plane stress assumption (wafer diameter \gg thickness), $\epsilon_{13} = \epsilon_{31} = 0$, so $\partial u_3 / \partial x_1$ represents the lattice tilt about x_2 axis, $\varphi(x_2)$, which is a minimum according to the strain map. This again confirms that lattice dilation/compression is the major form of effective misorientation in this wafer. The origin of the strain variation in this wafer is

believed to be the non-uniformity in nitrogen doping concentration. According to Jacobson's model,¹² when the isotropic lattice strain varies by $\Delta\epsilon = 3 \times 10^{-4}$ from one end of the wafer to another, the nitrogen doping concentration difference between the two ends will be at least $\Delta n = 6 \times 10^{18} \text{cm}^{-3}$, which is a reasonable value for heavily doped SiC crystals (10^{18} or 10^{19} level).

Similar analysis has been carried out on the second sample and four strain maps obtained from the two sets of $\pm \vec{g}$ contour maps recorded, as shown in Fig. 5a–d. With the reference point selected at the top-right corner of this 5 mm \times 5 mm sample, a strain center is observed. The strain value in this region goes as high as 4.704×10^{-3} for ϵ_{11} and almost doubled for ϵ_{22} (9.870×10^{-3}). The origin of this strain center is obviously the plastic deformation which occurred during the post-growth high-temperature heat treatment. Synchrotron white beam x-ray topograph (SWBXT) recorded from the same region confirms that a large numbers of basal plane dislocations (BPDs) have been nucleated and accumulated in the vicinity of heat center. The topographic image is shown in Fig. 6. The local BPD

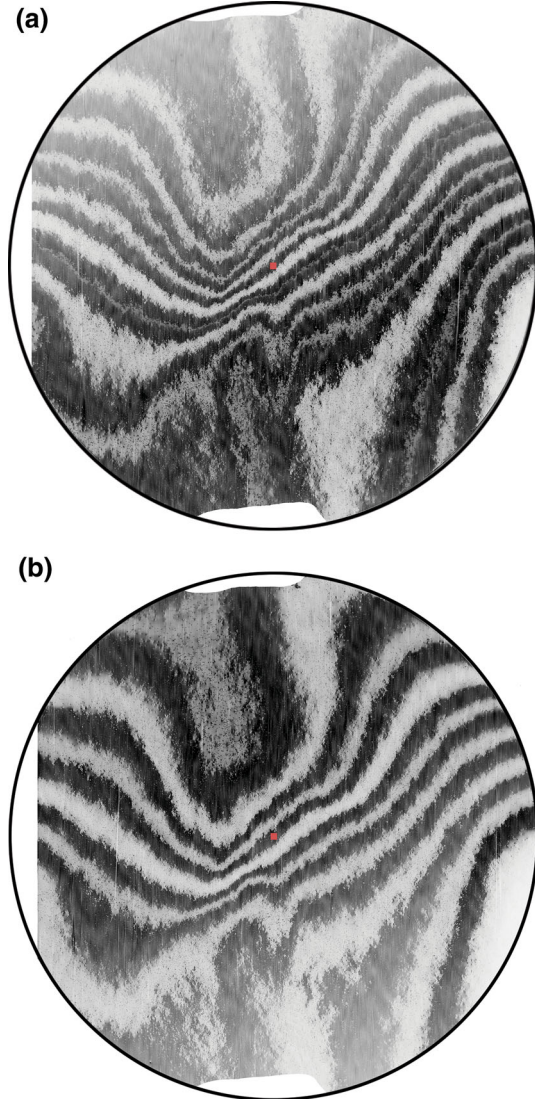


Fig. 3. Synchrotron double-crystal x-ray topographic contour maps with diffraction vector (a) $\vec{g} = (0008)$ and (b) $\vec{g} = (0008)$. Red dot denotes the reference point (Color figure online).

density near the strain center is above 10^5cm^{-2} level. Lattice distortion induced by these BPDs apparently causes the stress concentration. Again, the lattice tilt about x_2 and x_1 axes, $\partial u_1/\partial x_3$ and $\partial u_2/\partial x_3$ respectively, shows insignificant variations (10^{-5} level) compared to the normal strains according to the strain maps, indicating that the presence of dislocations mainly causes lattice dilation/compression instead of lattice tilt.

SUMMARY

A non-destructive method has been developed based on double-crystal x-ray topography to estimate the level and variation of lattice strain in 4H-SiC substrate crystals. This technique is capable of mapping different components of strain tensors at a

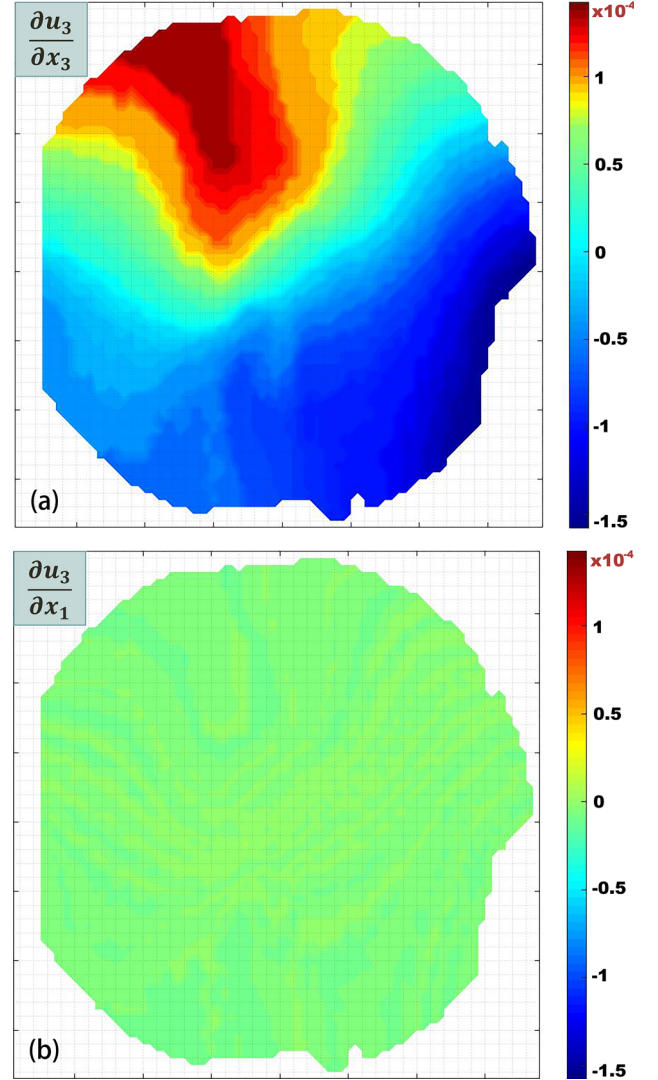


Fig. 4. Strain maps of different strain components: (a) $\partial u_3/\partial x_3$ and (b) $\partial u_3/\partial x_1$.

large scale (maximum 75 mm in diameter in APS), and the strain sensitivity is as good as the 10^{-6} level. Such a method is particular useful in revealing the strain field near stress centers and can be easily applied to different single-crystal substrate and epitaxy systems. The selection of the reference point is critical since the strain measured via this method is just relative values with respect to the reference point rather than the absolute strain. Demonstration of this technique shows that lattice dilation/compression, rather than lattice tilt, turns out to be the major type of deformation brought by both nitrogen dopants and BPDs.

ACKNOWLEDGEMENTS

This research used resources of the Advanced Photon Source, a U.S. Department of Energy (DOE) Office of Science User Facility operated for the DOE

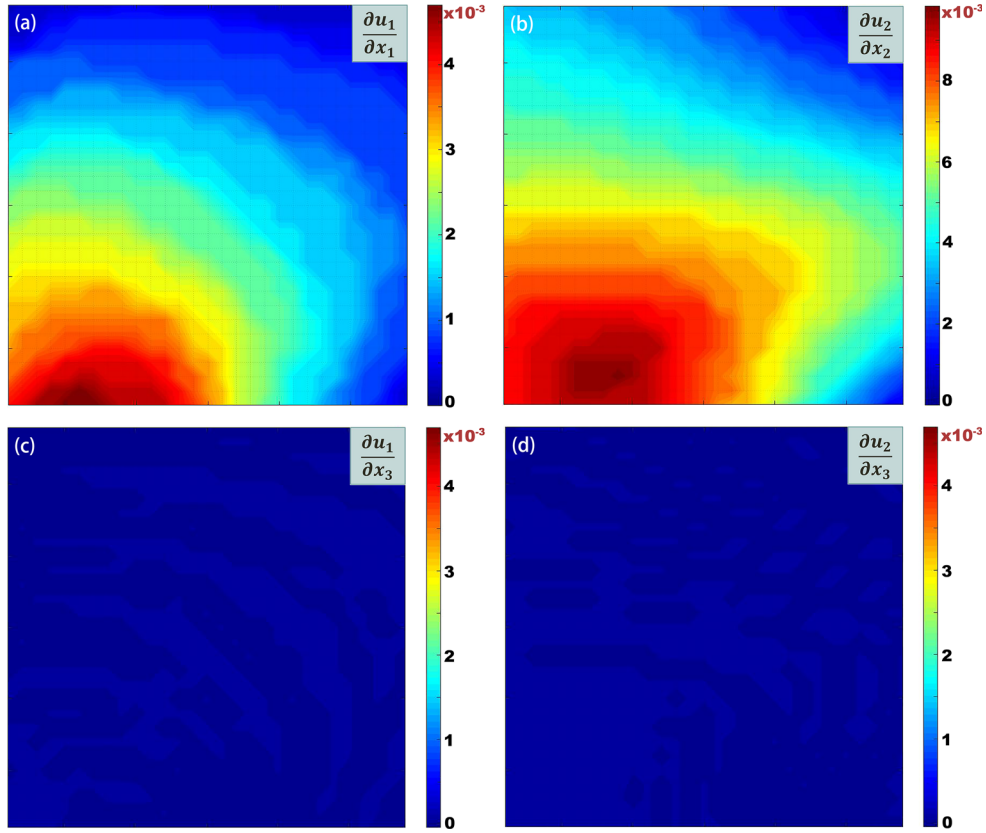


Fig. 5. Strain maps of four different strain components: (a) $\partial u_1/\partial x_1$ (b) $\partial u_2/\partial x_2$ (c) $\partial u_1/\partial x_3$ and (d) $\partial u_2/\partial x_3$.

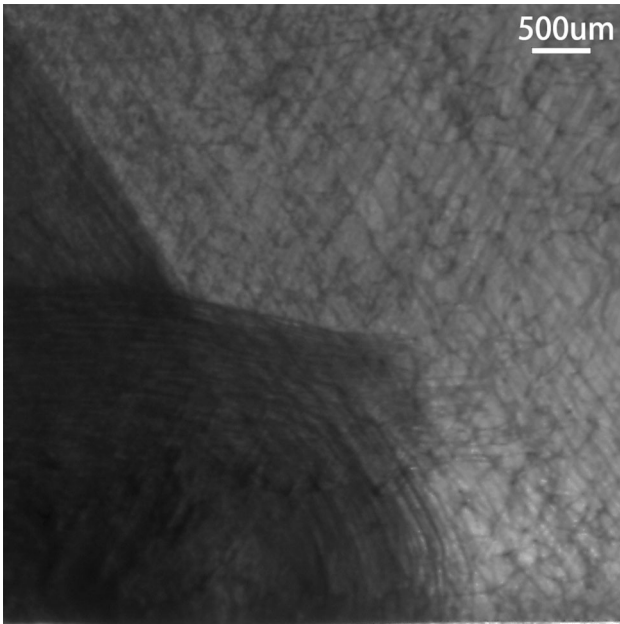


Fig. 6. SWBXT image recorded from the same sample showing the nucleation of large numbers of basal plane dislocations near the strain center. The density of dislocations is too high to resolve a single dislocation image.

Office of Science by Argonne National Laboratory under Contract No. DE-AC02-06CH11357. This work is based upon research conducted at the Cornell High Energy Synchrotron Source (CHESS) which is supported by the National Science Foundation and the National Institutes of Health/National Institute of General Medical Sciences under NSF award DMR-1332208. We would like to specially acknowledge Dr. Ken Finkelstein for his great help in experimental setup and useful discussion regarding this work. The Joint Photon Sciences Institute at SBU provided partial support for travel and subsistence for access to APS.

REFERENCES

1. E. Kasper, *Properties of Strained and Relaxed Silicon Germanium* (London: INSPEC, Institution of Electrical Engineers, 1995).
2. D.K. Bowen and S.T. Davies, *Nucl. Instrum. Methods Phys. Res.* 208, 725 (1983).
3. S. Kikuta, K. Kohra, and Y. Sugita, *Jpn. J. Appl. Phys.* 5, 1047 (1966).
4. S.J. Barnett, B.K. Tanner, and G.T. Brown, *MRS Symp. Proc.* 41, 83 (1985).
5. C. Ferrari, D. Korytar, and J. Kumar, *IL Nuovo Cimento D* 19, 165 (1997).
6. S.R. Stock, H. Chen, and H.K. Birnbaum, *Philos. Mag. A* 53, 73 (1986).

Mapping of Lattice Strain in 4H-SiC Crystals by Synchrotron Double-Crystal X-ray Topography

7. D.J. Larson Jr, R.P. Silberstein, D. DiMarzio, F.C. Carlson, D. Gillies, G. Long, M. Dudley, and J. Wu, *Semicond. Sci. Technol.* 8, 911 (1993).
8. M. Jackson, M.S. Goorsky, A. Noori, S. Hayashi, R. Sandhu, B. Poust, P. Chang-Chien, A. Gutierrez-Aitken, and R. Tsai, *Phys. Status Solidi A* 204, 2675 (2007).
9. A.T. Macrander, S. Krasnicki, Y. Zhong, J. Maj, and Y. Chu, *Appl. Phys. Lett.* 87, 194113 (2005).
10. G. Yang, R. Jones, F. Klein, K. Finkelstein, and K. Livingston, *Diam. Relat. Mater.* 19, 719 (2010).
11. S. Stoupin, Y. Shvyd'ko, E. Trakhtenberg, Z. Liu, K. Lang, X. Huang, M. Wiczorek, E. Kasman, J. Hammonds, A. Macrander, and L. Assoufid, *AIP Conf Proc* 1741, 050020 (2016).
12. H. Jacobson, J. Birch, C. Hallin, A. Henry, R. Yakimova, T. Tuomi, and E. Janzén, *Appl. Phys. Lett.* 82, 3689 (2003).